

High-resolution hyperfine spectroscopy of excited states using electromagnetically-induced transparency

ANUSHA KRISHNA, KANHAIYA PANDEY, AJAY WASAN, AND VASANT NATARAJAN (*)
Department of Physics, Indian Institute of Science, Bangalore 560 012, INDIA

PACS. 32.10.Fn – Fine and hyperfine structure.

PACS. 42.50.Gy – Effects of atomic coherence on propagation, absorption, and amplification of light.

PACS. 42.50.-p – Quantum optics.

Abstract. – We use the phenomenon of electromagnetically-induced transparency in a three-level atomic system for hyperfine spectroscopy of upper states that are not directly coupled to the ground state. The three levels form a ladder system: the probe laser couples the ground state to the lower excited state, while the control laser couples the two upper states. As the frequency of the control laser is scanned, the probe absorption shows transparency peaks whenever the control laser is resonant with a hyperfine level of the upper state. As an illustration of the technique, we measure hyperfine structure in the $7S_{1/2}$ states of ^{85}Rb and ^{87}Rb , and obtain an improvement of more than an order of magnitude over previous values.

The use of coherent-control techniques in three-level systems is now an important tool for modifying the absorption properties of a weak probe laser [1, 2, 3]. For example, in the phenomenon of electromagnetically induced transparency (EIT), an initially absorbing medium is made transparent to a probe beam when a strong control laser is switched on [4, 5]. EIT techniques have several practical applications in probe amplification [6], lasing without inversion [7], and suppression of spontaneous emission [3, 8, 9, 10]. Experimental observations of EIT have been mainly done using alkali atoms (such as Rb and Cs), where the transitions have strong oscillator strengths and can be accessed with low-cost tunable diode lasers.

In this paper, we use the phenomenon of EIT in a novel application, namely high-resolution spectroscopy of hyperfine structure in excited states. The experiments are done in a ladder system, where the control laser drives the upper transition and the probe laser measures absorption on the lower transition. In normal EIT experiments, the frequency of the probe laser is scanned while the frequency of the control laser is kept fixed. By contrast, in our technique, it is the frequency of the control laser that is scanned while the probe laser remains locked on resonance. The probe-absorption signal then shows transparency peaks every time the control laser comes into resonance with a hyperfine level of the excited state.

Measurement of hyperfine structure in excited states is important because these states are used in diverse experiments ranging from atomic signatures of parity non-conservation (PNC)

(*) E-mail: vasant@physics.iisc.ernet.in

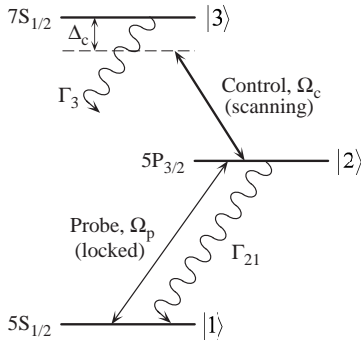


Fig. 1

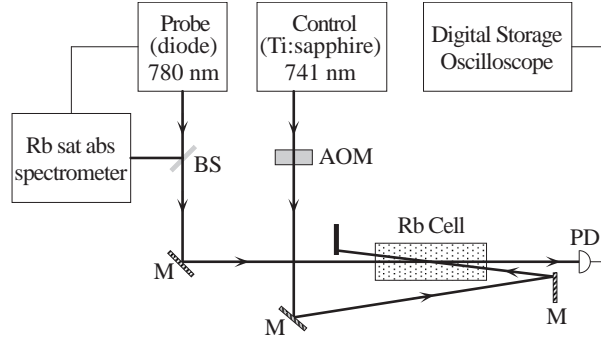


Fig. 2

Fig. 1 – Three-level ladder system in Rb. The probe laser has Rabi frequency Ω_p and is locked to the lower transition. The control laser has Rabi frequency Ω_c and is scanned across the upper transition with a detuning Δ_c .

Fig. 2 – Schematic of the experiment. The control beam after the AOM consists of two parts, one at the laser frequency and one shifted by the rf frequency. The angle between the beams in the vapor cell has been exaggerated for clarity, in reality it is less than 10 mrad. Figure key: Sat. abs., saturated absorption; BS, beam splitter; M, mirror; AOM, acousto-optic modulator; PD, photodiode.

to resonance ionization mass spectrometry [11]. For example, the $7S$ state in Cs has been used for the most sensitive test of atomic PNC to date [12]. However, to convert the experimental results into useful information about the parity-violating weak interaction, the data has to be compared to complex theoretical calculations in Cs. Knowledge of hyperfine structure thus provides valuable information about the structure of the nucleus (nuclear deformation) and its influence on the atomic wavefunction. Hyperfine spectroscopy on these excited states is complicated by the fact that they have the same parity as the ground state and can only be accessed through weak two-photon transitions. By contrast, our technique provides strong, easily-measured signals. In addition, there is an interesting narrowing of the linewidth in room-temperature vapor by the use of counter-propagating beams, which is important for high accuracy in the measurement. As an illustration of the power of this technique, we have used it to measure hyperfine structure in the $7S_{1/2}$ state of Rb, and demonstrate an improvement of more than an order of magnitude in precision over previous values.

The ladder system in Rb is shown in Fig. 1. The levels $|1\rangle$, $|2\rangle$, and $|3\rangle$, are the $5S_{1/2}$, $5P_{3/2}$, and $7S_{1/2}$ states, respectively. The probe laser is tuned to the lower $5S_{1/2} \leftrightarrow 5P_{3/2}$ transition at 780 nm with a Rabi frequency of Ω_p . The spontaneous decay rate from this state (Γ_{21}) is 6 MHz. The control laser is tuned to the upper $5P_{3/2} \leftrightarrow 7S_{1/2}$ transition at 741 nm with a detuning of Δ_c and Rabi frequency of Ω_c . The spontaneous decay from this state back to the ground state is primarily through the cascade $7S \rightarrow 6P \rightarrow 5S$ transition. The decay rate Γ_3 is 11 MHz.

The experimental set up is shown schematically in Fig. 2. The probe beam is derived from a feedback-stabilized diode laser system operating at 780 nm [13]. The linewidth of the laser after stabilization is less than 500 kHz. The probe beam has $1/e^2$ diameter of 2 mm. The control beam comes from a ring-cavity Ti:Sapphire laser tuned to 741 nm. The Ti:S laser is stabilized to an ovenized reference cavity that gives it an instantaneous linewidth of 500 kHz. The control beam consists of two parts, one at the laser frequency and one that is frequency shifted using an acousto-optic modulator (AOM). As discussed later, the AOM-shifted beam

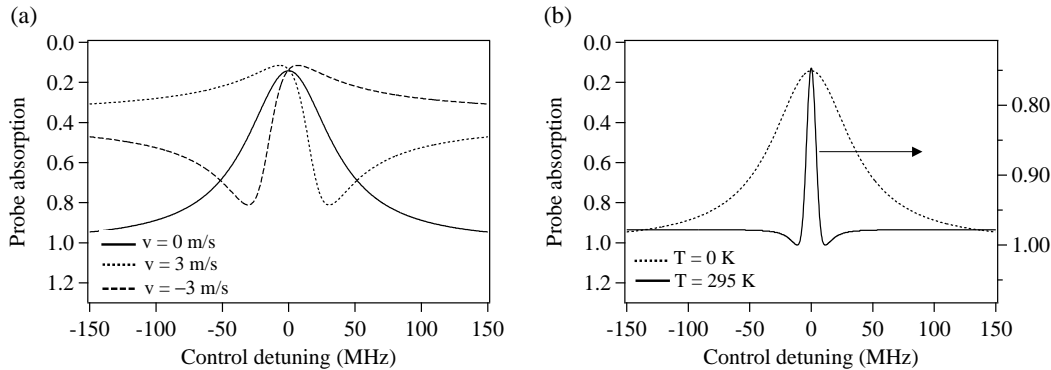


Fig. 3 – Theoretical lineshapes for probe absorption. In (a), we show the normalized absorption curves with $\Delta_p = 0$ and $\Omega_c = 20$ MHz, for zero-velocity atoms and atoms moving with $v = \pm 3$ m/s. In (b), we show the effect of thermal averaging: the linewidth is reduced significantly at $T = 295$ K compared to $T = 0$ K. The scale of the transparency is also reduced, as seen from the right axis for the $T = 295$ K curve. Note the inverted y -axes in both graphs.

is used for calibrating the frequency-scan axis. One important experimental requirement is to double pass through the AOM so that the unshifted (zeroth-order) and shifted beams propagate in the same direction. This ensures that the two components are mixed perfectly and there is no angle between them. The control beam is similar to the probe beam and has a diameter of 2 mm. The beam counter-propagates with respect to the probe beam through a room-temperature vapor cell containing Rb. The absorption through the cell is about 25%. The two beams have identical polarization and the angle between them is less than 10 mrad.

We first consider the theoretical analysis of probe absorption in a ladder system in the presence of the control laser. In the weak probe limit, the absorption of the probe is proportional to $\text{Im}(\rho_{21})$, where ρ_{21} is the induced polarization on the $|1\rangle \leftrightarrow |2\rangle$ transition coupled by the laser. From the density-matrix equations, the steady-state value of ρ_{21} is given by [14]:

$$\rho_{21} = -\frac{i(\Omega_p/2)}{\left(\frac{\Gamma_{21}}{2} - i\Delta_p\right) + \frac{\Omega_c^2/4}{\Gamma_{3/2} - i(\Delta_p + \Delta_c)}} \quad (1)$$

where Δ_p is the detuning of the probe from resonance. The calculated absorption curve (note the inverted y -axis) for $\Delta_p = 0$ and $\Omega_c = 20$ MHz is shown in Fig. 3(a) as a function of Δ_c . The absorption is normalized to a value of 1 in the absence of the control laser. There is a distinct EIT peak at line center: the absorption falls by about 80% when the control laser is exactly on resonance. However, the linewidth of the transparency peak is quite large, with a value of about 70 MHz for $\Omega_c = 20$ MHz.

The above analysis is correct for a stationary atom. In a room-temperature vapor, we have to account for the thermal velocity distribution. For an atom moving with a velocity v in the same direction as the probe beam, the probe detuning decreases to $\Delta_p - v/\lambda_p$, while the control detuning increases to $\Delta_c + v/\lambda_c$ due to the counter-propagating configuration. Here, $\lambda_{p,c}$ are the respective center wavelengths for the two transitions. The resulting absorption curves for $v = 3$ m/s and $v = -3$ m/s are also shown in Fig. 3(a). The curve has a dispersive lineshape, and shows increased absorption on one side of line center. More importantly, it is slightly asymmetric because of the unequal values of λ_p and λ_c , i.e., for a given velocity, the detuning changes by different amounts for the probe and the control.

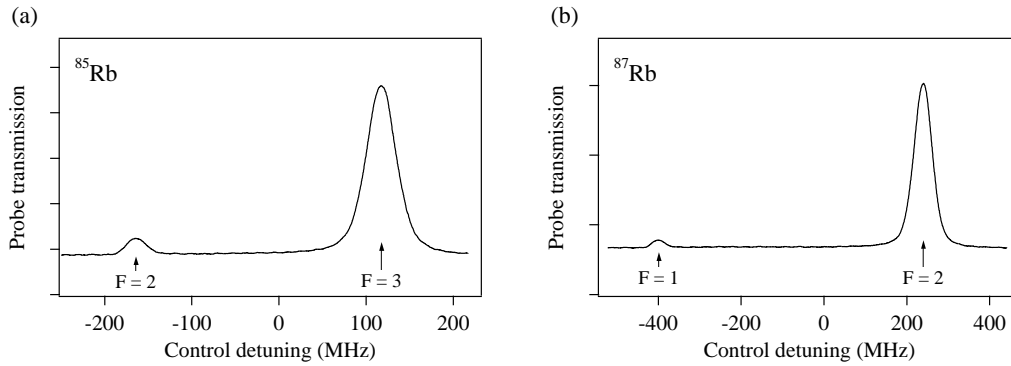


Fig. 4 – Experimental EIT peaks in Rb. In (a), we show the probe transmission as a function of control detuning in ^{85}Rb . The transparency peaks correspond to the two hyperfine levels labelled by their F values. Control detuning is measured from the unperturbed $7S_{1/2}$ state. In (b), we show the corresponding spectrum in ^{87}Rb .

The effect of this for a Maxwell-Boltzmann velocity distribution is seen in Fig. 3(b). The two absorption curves shown are for $T = 0$ K and $T = 295$ K. The interesting feature is that the linewidth of the curve for room-temperature atoms is significantly *reduced* by thermal averaging; the use of a counter-propagating geometry *decreases* the linewidth from 70 MHz for zero-temperature atoms to 17 MHz for room-temperature atoms. The narrowing is advantageous because it allows us to measure hyperfine intervals with greater precision. However, the narrowing is accompanied by a decrease in the scale of the transparency, with only 25% reduction in absorption at line center. Note also the slight lineshape distortion for room-temperature atoms, where the absorption increases slightly before approaching an asymptotic value. The cause for this is again the asymmetric detuning of the control and probe for a given velocity. The distortion disappears when the value of Ω_c increases beyond 100 MHz. Higher values of Ω_c also result in power broadening of the linewidth, to about 50 MHz for $\Omega_c = 100$ MHz. Finally, because we are considering a fixed frequency for the probe beam, the spectrum has a flat background (corresponding to absorption by the zero-velocity atoms) and changes only when the control beam is close to resonance. This is different from other high-resolution spectroscopy techniques in room-temperature vapor, such as saturated-absorption spectroscopy, where the spectrum shows an underlying Doppler profile.

We now consider experimental spectra in ^{85}Rb . The $7S_{1/2}$ state has two hyperfine levels: $F = 2$ and 3 with an interval of 282 MHz. The probe laser is locked to the $F = 3 \rightarrow 3$ hyperfine peak of the lower transition and has a power of 2 mW. The measured probe transmission spectrum is shown in Fig. 4(a). As the control laser is scanned, there are two distinct transparency peaks corresponding to the two hyperfine levels. The linewidth of the peaks is about 50 MHz, which is the theoretically predicted linewidth at room temperature for a Rabi frequency of 100 MHz. Note that the corresponding linewidth at $T = 0$ would be about 1500 MHz. The value of $\Omega_c = 100$ MHz is consistent with the control power of 100 mW used for this experiment. A similar spectrum for ^{87}Rb is shown in Fig. 4(b), measured with the probe laser locked to the $F = 2 \rightarrow 2$ hyperfine peak. Note that the two hyperfine levels ($F = 1, 2$) in this case have a larger separation of 638 MHz.

For the measurement of the hyperfine interval, there are two points to note from the experimental curves. The first is that we need a precise calibration of the frequency-scan axis of the control laser. The second is that the height of the two peaks is very different. Therefore,

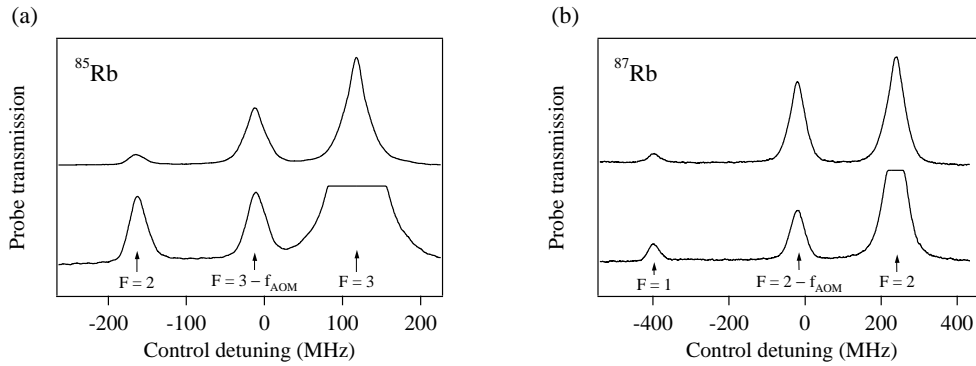


Fig. 5 – Hyperfine measurement using AOM shifting. In (a), the upper trace is the probe transmission in ^{85}Rb in the presence of the AOM-shifted control beam. The new peak in the middle is the frequency-shifted twin of the $F = 3$ peak, allowing precise calibration of the scan axis. The bottom trace is obtained by reducing the rf power into the AOM and increasing the photodiode gain so that the smaller peaks are comparable. In (b), we show a similar set of curves for ^{87}Rb .

the measurement proceeds as follows. The scan calibration is achieved by using the AOM-shifted control beam, as shown in the experimental schematic (Fig. 2). In the presence of both control beams, the larger peak shows a twin peak at a location down-shifted by the AOM frequency. The resulting spectrum of three peaks for ^{85}Rb is shown in the upper trace of Fig. 5(a). Note that the smaller peak also has a twin which will appear to its left, but this is very small and not shown. Since the distance between the primary peak and its twin is exactly the AOM frequency, this allows us to calibrate the frequency axis precisely. Now, the rf power into the AOM is reduced so that the AOM-shifted peak becomes comparable in height to the smaller peak, and simultaneously the gain of the photodiode amplifier is increased. The resulting spectrum is shown in the lower trace Fig. 5(a). The calibrated distance between the smaller peak and the AOM-shifted peak is then used to determine the hyperfine interval. Note that the primary peak saturates the amplifier, but this is not important since it is not used in the hyperfine measurement. In other words, the two large peaks in the upper trace are used for calibration, while the two smaller peaks in the lower trace are used for the measurement. A similar set of curves for ^{87}Rb is shown in Fig. 5(b).

The primary advantage of this procedure is that the error in determining the peak position is reduced. To the extent that the two peaks are similar, any systematic error in determining the peak centers will cancel when taking the difference. The peak centers are determined in two ways: first by a peak-fitting routine, and then by determining the zero crossing of the numerical third derivative. This gives the peak position with a typical error of about 10 kHz.

Before we turn to the results, let us consider the sources of error in the technique. An important consideration is a systematic shift of the probe laser from resonance due to effects such as stray magnetic fields in the vicinity of the vapor cell, phase shifts in the feedback loop, and background collisions. However, it is important to note that this will not affect the measurement of the hyperfine interval at all. In other words, such a shift is equivalent to a detuning of the probe from resonance, and it can be shown from Eq. 1 that a non-zero value of Δ_p will simply shift the location of the transparency peak by this amount in the opposite direction. Hence, both peaks in Fig. 3 will shift by the same amount and the hyperfine interval will be unaffected.

Similarly, the effect of an angle between the probe and control beams is unimportant.

TABLE I – *Hyperfine-interval measurements using different AOM offsets in ^{85}Rb and ^{87}Rb .*

Hyperfine interval ^{85}Rb	AOM offset (MHz)	Value (MHz)	Hyperfine interval ^{87}Rb	AOM offset (MHz)	Value (MHz)
$F = 3 - F = 2$	130.021	282.280	$F = 2 - F = 1$	180.015	638.213
	142.001	282.210		190.046	638.266
	154.012	282.277		200.076	638.338
	166.005	282.224		240.145	638.330
	178.093	282.297		250.106	638.303
	190.017	282.291		270.198	638.578

Such an angle implies that the two beams come into simultaneous resonance with a non-zero velocity group. Since the velocity can be either positive or negative, this only causes a small broadening of the EIT peak but does not affect the peak center. Indeed, we have seen that there is no measurable change in the linewidth of the theoretical curves shown in Fig. 3(b) for a misalignment angle of 10 mrad, which is the maximum value of the angle between our beams. However, there could be a systematic shift of line center if there is velocity redistribution due to radiation pressure effects, but this should be the same for both peaks and cancel in a difference measurement. In a similar manner, shifts due to collisions will affect both peaks equally and cancel in the difference.

Thus the main sources of error in our technique arise due to residual nonlinearity of the frequency-scan axis, and the accuracy in determining the peak centers. To check for these errors, we have repeated the measurements at various values of the AOM frequency. A representative list of 6 measurements to show the range of AOM frequencies is given in Table I. The final values are obtained by taking an average of all the measurements and calculating the error in the mean. From a total of about 60 measurements in ^{85}Rb and 40 measurements in ^{87}Rb repeated over a period of several days, we obtain the following average values for the hyperfine interval:

$$\begin{aligned} ^{85}\text{Rb}: \{F = 3 - F = 2\} &= 282.254(54) \text{ MHz}, \\ ^{87}\text{Rb}: \{F = 2 - F = 1\} &= 638.347(90) \text{ MHz}. \end{aligned}$$

The quoted errors include a systematic error of 40 kHz to account for unknown sources of error. The larger error in ^{87}Rb is because of the larger interval being measured, requiring larger extrapolation of the scan axis. The measured interval can be used to calculate the value of the magnetic-dipole coupling constant A in the $7S_{1/2}$ state as:

$$\begin{aligned} ^{85}\text{Rb}: A &= 94.085(18) \text{ MHz}, \\ ^{87}\text{Rb}: A &= 319.174(45) \text{ MHz}. \end{aligned}$$

These values are compared with the recommended values from Ref. [15] in Fig. 6. As can be seen, the values are consistent, but the accuracy is improved considerably, by a factor of 35 in ^{85}Rb and by a factor of 71 in ^{87}Rb .

In summary, we have demonstrated a new technique for high-resolution hyperfine measurements in excited states using the phenomenon of electromagnetically-induced transparency. The experiments have been done using a ladder system in atomic Rb. The weak probe laser is locked to the lower transition while the strong control laser is scanned across the upper transition. Transparency peaks appear in the probe transmission whenever the control laser comes into resonance with a hyperfine level. The frequency axis of the control laser is set by

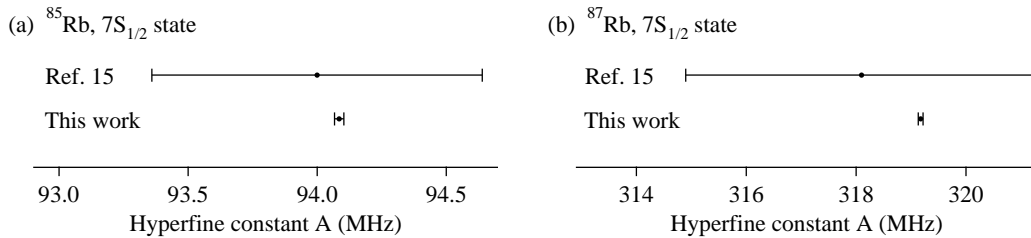


Fig. 6 – Comparison of hyperfine constants. In (a), we compare the value of A in ^{85}Rb measured in this work to the value from Ref. [15]. In (b), we show a similar comparison for ^{87}Rb .

using an AOM-shifted beam with a known frequency offset. In this manner, we are able to measure hyperfine intervals in the $7S_{1/2}$ state of Rb with an error of less than 100 kHz. This is already a considerable improvement over previous measurements, but we have not really pushed the limits of accuracy of this technique. For example, we have recently demonstrated a technique for measurement of hyperfine intervals with 20 kHz accuracy using an AOM whose frequency is locked to the hyperfine interval of interest [16]. This will eliminate any potential errors due to nonlinearity of the scan. Using this method, we hope to be able to further improve the accuracy of the current technique. We plan to measure excited-state hyperfine structure in other atoms that are of interest for PNC measurements, such as Cs and Yb [17].

* * *

We thank Anand Ramanathan for help with the experiments. This work was supported by the Department of Science and Technology, Government of India. One of us (A.W.) acknowledges financial support from CSIR, India.

REFERENCES

- [1] L. M. Narducci *et al.*, Phys. Rev. A **42**, 1630 (1990).
- [2] G. Vemuri, G. S. Agarwal, and B. D. N. Rao, Phys. Rev. A **53**, 2842 (1996).
- [3] U. D. Rapol, A. Wasan, and V. Natarajan, Phys. Rev. A **67**, 053802 (2003).
- [4] K.-J. Boller, A. Imamoglu, and S. E. Harris, Phys. Rev. Lett. **66**, 2593 (1991).
- [5] S. E. Harris, Phys. Today **50**, 36 (1997).
- [6] S. Menon and G. S. Agarwal, Phys. Rev. A **61**, 013807 (2000).
- [7] A. S. Zibrov *et al.*, Phys. Rev. Lett. **75**, 1499 (1995).
- [8] D. J. Gauthier, Y. Zhu, and T. W. Mossberg, Phys. Rev. Lett. **66**, 2460 (1991).
- [9] S.-Y. Zhu, L. M. Narducci, and M. O. Scully, Phys. Rev. A **52**, 4791 (1995).
- [10] S.-Y. Zhu and M. O. Scully, Phys. Rev. Lett. **76**, 388 (1996).
- [11] M. G. Payne, L. Deng, and N. Thonnard, Rev. Sci. Instrum. **65**, 2433 (1994).
- [12] C. S. Wood *et al.*, Science **275**, 1759 (1997).
- [13] A. Banerjee, U. D. Rapol, A. Wasan, and V. Natarajan, Appl. Phys. Lett. **79**, 2139 (2001).
- [14] J. Gea-Banacloche, Y. Li, S. Jin, and M. Xiao, Phys. Rev. A **51**, 576 (1995).
- [15] E. Arimondo, M. Inguscio, and P. Violino, Rev. Mod. Phys. **49**, 31 (1977).
- [16] U. D. Rapol, A. Krishna, and V. Natarajan, Eur. Phys. J. D **23**, 185 (2003).
- [17] V. Natarajan, Eur. Phys. J. D **32**, 33 (2005).